University of South Carolina
Scholar Commons

Faculty Publications | Chemical Engineering, Department of

4-1-2021

Hydrothermal Synthesis and Structural Investigation of a Crystalline Uranyl Borosilicate

Kristen A. Pace
Center for Hierarchical Waste Form Materials

Vladislav V. Klepov
University of South Carolina

Mark D. Smith
University of South Carolina - Columbia, mdsmith3@mailbox.sc.edu

Travis Williams
University of South Carolina

Gregory Morrison
Center for Hierarchical Waste Form Materials

See next page for additional authors

Follow this and additional works at: https://scholarcommons.sc.edu/eche_facpub

Part of the Biochemical and Biomolecular Engineering Commons

Publication Info

Inorganics, Issue 4, 2021.

This Article is brought to you by the Chemical Engineering, Department of at Scholar Commons. It has been accepted for inclusion in Faculty Publications by an authorized administrator of Scholar Commons. For more information, please contact digres@mailbox.sc.edu.

Author(s)
Kristen A. Pace, Vladislav V. Klepov, Mark D. Smith, Travis Williams, Gregory Morrison, Jochen A. Lauterbach, Scott T. Misture, and Hans Conrad Zur Loye

This article is available at Scholar Commons: https://scholarcommons.sc.edu/eche_facpub/1132

inorganics

MDPI

Article

Hydrothermal Synthesis and Structural Investigation of a Crystalline Uranyl Borosilicate

Kristen A. Pace [1,2,†], Vladislav V. Klepov [2,‡], Mark D. Smith [2], Travis Williams [3], Gregory Morrison [1,2], Jochen A. Lauterbach [3], Scott T. Misture [1,4] and Hans-Conrad zur Loye [1,2,*]

1 Center for Hierarchical Waste form Materials, Columbia, SC 29208, USA; kpace@lanl.gov (K.A.P.); MORRI383@mailbox.sc.edu (G.M.); misture@alfred.edu (S.T.M.)
2 Department of Chemistry and Biochemistry, University of South Carolina, Columbia, SC 29208, USA; klepov@northwestern.edu (V.V.K.); MDSMITH3@mailbox.sc.edu (M.D.S.)
3 Department of Chemical Engineering, University of South Carolina, Columbia, SC 29208, USA; traswill@gmail.com (T.W.); LAUTERAJ@cec.sc.edu (J.A.L.)
4 Kazuo Inamori School of Engineering, Alfred University, Alfred, NY 14802, USA
* Correspondence: zurloye@mailbox.sc.edu
† Present Address: Pit Technologies Division, Los Alamos National Laboratory, Los Alamos, NM 87545, USA.
‡ Present Address: Department of Chemistry, Northwestern University, Evanston, IL 60208, USA.

Abstract: The relevance of multidimensional and porous crystalline materials to nuclear waste remediation and storage applications has motivated exploratory research focused on materials discovery of compounds, such as actinide mixed-oxoanion phases, which exhibit rich structural chemistry. The novel phase $K_{1.8}Na_{1.2}[(UO_2)BSi_4O_{12}]$ has been synthesized using hydrothermal methods, representing the first example of a uranyl borosilicate. The three-dimensional structure crystallizes in the orthorhombic space group *Cmce* with lattice parameters a = 15.5471(19) Å, b = 14.3403(17) Å, c = 11.7315(15) Å, and V = 2615.5(6) Å^3, and is composed of UO_6 octahedra linked by $[BSi_4O_{12}]^{5-}$ chains to form a $[(UO_2)BSi_4O_{12}]^{3-}$ framework. The synthesis method, structure, results of Raman, IR, and X-ray absorption spectroscopy, and thermal stability are discussed.

Keywords: crystalline borosilicate; actinides; supercritical hydrothermal synthesis; waste forms

check for updates

Citation: Pace, K.A.; Klepov, V.V.; Smith, M.D.; Williams, T.; Morrison, G.; Lauterbach, J.A.; Misture, S.T.; zur Loye, H.-C. Hydrothermal Synthesis and Structural Investigation of a Crystalline Uranyl Borosilicate. *Inorganics* **2021**, *9*, 25. https://doi.org/10.3390/inorganics9040025

Academic Editor: Duncan H. Gregory

Received: 5 March 2021
Accepted: 29 March 2021
Published: 6 April 2021

Publisher's Note: MDPI stays neutral with regard to jurisdictional claims in published maps and institutional affiliations.

Copyright: © 2021 by the authors. Licensee MDPI, Basel, Switzerland. This article is an open access article distributed under the terms and conditions of the Creative Commons Attribution (CC BY) license (https://creativecommons.org/licenses/by/4.0/).

1. Introduction

In the U.S., alkali borosilicate glasses are used as a primary nuclear waste form material for the immobilization of high-level waste. The glasses are durable and can host a wide range of elements in the disordered structures, which are composed of network forming SiO_4 and BO_4 tetrahedra as well as trigonal planar BO_3 anions that support compositional variety [1]. However, the low solubility of actinides in glasses with high actinide loadings has motivated researchers to study the crystal chemistry of actinide compounds, both to identify phases that may be forming under simulated conditions and to develop an understanding of the fundamental chemistry of waste form relevant phases [2,3]. Moreover, it has been recognized that for some waste streams, crystalline waste forms may offer an advantage over glasses such as higher waste loading capacities [4,5]. The structural complexity exhibited by multidimensional and porous crystalline materials can also be exploited, enabling the incorporation of specific radionuclides and, in some cases, ion exchange capabilities [6–8].

Among the many compound classes that have been studied for waste form applications, uranyl silicates and borates have received considerable attention. The variable arrangement of SiO_4 tetrahedra in uranyl silicate compounds has resulted in a multitude of different structure types, many of which are three-dimensional [9–17]. Likewise, the ability of BO_3 and BO_4 units to polymerize to form polyborate units has given rise to a rich structural chemistry in uranyl borates [3,18–24]. It is therefore unsurprising that incorporation of mixed-oxoanions into the structures of uranyl compounds often facilitates further

structural diversity. For example, a few uranyl borophosphate [25,26], borogermanate [27], aluminoborate [28], and aluminophosphate [29] compounds are known, most of which exhibit complex open-framework structures. No such uranyl compounds containing borosilicate units have been reported, although there are several existing non-uranyl compounds exhibiting a variety of different borosilicate units. While uranyl borosilicates are relevant to waste form applications, in the case of non-actinide borosilicates, the structural diversity afforded by the presence of the borosilicate units often promotes the formation of noncentrosymmetric structures, making some of these compounds potentially promising candidates as nonlinear optical materials [30]. Some of the known examples within these compound classes contain isolated BO_3 and SiO_4 structural units [31,32], condensed BO_4 and SiO_4 tetrahedra [33,34], trigonal planar BO_3 units condensed with tetrahedral BO_4 and SiO_4 [35], as well as HBO_4 and SiO_4 hydroxyborosilicate units [36].

Herein, we present the first example of a uranyl borosilicate compound, $K_{1.8}Na_{1.2}[(UO_2)BSi_4O_{12}]$, which was synthesized using hydrothermal synthesis methods with supercritical water as the reaction medium. The structure of the compound was investigated, revealing residual electron density near the uranyl oxygen that was attributed to either the presence of a light atom in an unusual coordination or to an unidentified crystal defect, prompting further investigation of the compound using a combination of X-ray absorption and vibrational spectroscopy techniques, characterization of its thermal properties, as well as the employment of first principles calculations to determine the optimized geometry of the uranium coordination environment [37,38]. Using single crystal X-ray diffraction, the compound was found to crystallize in a centrosymmetric structure type with a complex three-dimensional crystal structure containing unique $[BSi_4O_{12}]^{5-}$ chains composed of BO_4 and SiO_4 tetrahedra. Characterizations of the thermal and spectroscopic properties were performed using thermogravimetric analysis in addition to Raman, IR, and extended X-ray absorption fine structure spectroscopy. These data, in addition to the results of first principles calculations, suggest that the residual electron density in the structure is likely due to a crystal defect. The successful preparation of $K_{1.8}Na_{1.2}[(UO_2)BSi_4O_{12}]$ serves to further expand on the diverse structural chemistry of uranium and moreover, highlights an under-explored set of synthetic conditions that may be exploited to obtain other novel actinide borosilicate compounds.

2. Materials and Methods

2.1. Reagents

$UO_3 \cdot xH_2O$ (International Bio-Analytical Industries, ACS grade), $NaBO_2 \cdot 4H_2O$ (Acros Organics, 98.5%), SiO_2 (Alfa Aesar, 99.9%), KOH pellets (Alfa Aesar, 99.99%), and KOH solution (Fisher Scientific, 45% *w*/*w*) were used as received. Caution: although the uranium precursors used contain depleted uranium, standard safety procedures for handling radioactive materials must be followed.

2.2. Synthesis

$UO_3 \cdot xH_2O$ (150.3 mg), $NaBO_2 \cdot 4H_2O$ (689.3 mg), and SiO_2 (300.4 mg) were added to a mineralizer solution of aqueous KOH (224.4 mg in 2 mL deionized water) in an approximate molar ratio of 1:10:10:8 of U:Na,B:Si:K. A 5% by mass excess of $UO_3 \cdot xH_2O$ was added to the reaction mixture to compensate for the unknown degree of hydration of the uranium starting material. The mixture was sealed in a 12.7 cm silver tube that was loaded into a high-pressure vessel containing approximately 20 mL of water to serve as counterpressure. The vessel was placed in a programmable oven and heated to 400 °C for 48 h, followed by a period of slow cooling to 350 °C at a rate of 3 °C per hour. The vessel was then allowed to naturally cool to room temperature. An estimated 30 MPa of pressure was generated during the reaction based on the pressure-temperature diagram of water.

Upon cooling, the silver tube was cut open and the mother liquor was decanted. The contents of the tube were sonicated in deionized water prior to vacuum filtering and thoroughly washing the products in water and acetone. The product mixture consisted of

brown/black polycrystalline powders of unknown composition in addition to clusters of large yellow prismatic crystals (Figure S1) in approximately 70% yield. The large yellow prismatic crystals were manually separated from the product mixture and ground to a powder to obtain a phase pure sample for bulk property measurements.

To obtain high quality single crystals suitable for single crystal X-ray diffraction measurements, efforts were made to optimize the reaction conditions by varying the hydroxide concentration. In order to have more precise control over the KOH concentration, subsequent attempts employed identical reaction conditions with substitution of KOH pellets for KOH solution diluted from a 45% w/w stock solution. Reactions containing 2 mL of 2M KOH solution (1:10:10:8 = U:Na,B:Si:K) resulted only in the formation of brown polycrystalline material, identified as a mixture of $K(UO)Si_2O_6$ [17] and $Na_7UO_2(UO)_2(UO_2)_2Si_4O_{16}$ [39] via powder X-ray diffraction. In comparison, reactions containing 2 mL of 1.5M KOH solution (1:10:10:6 = U:Na,B:Si:K) resulted in polycrystalline $Na_7UO_2(UO)_2(UO_2)_2Si_4O_{16}$ along with an approximately 40% yield of high quality single crystals of $K_{1.8}Na_{1.2}[(UO_2)BSi_4O_{12}]$ that were used for single crystal X-ray analysis.

2.3. Single Crystal X-ray Diffraction

Single crystal X-ray diffraction data were collected at 301(2) K using a Bruker D8 QUEST diffractometer equipped with an Incoatec microfocus source (Mo Kα radiation, λ = 0.71073 Å). Data were integrated and corrected for absorption effects using SAINT+ and SADABS programs [40]. An initial structure model was obtained with SHELXT and subsequently refined with SHELXL-2018 using the ShelXle interface [41,42]. The ADDSYM program implemented into PLATON software was used to check for possible missing symmetry, and no alternative symmetry was found [43]. Crystallographic data for $K_{1.8}Na_{1.2}[(UO_2)BSi_4O_{12}]$ are provided in Table 1. A residual electron density peak of 4.17 e/Å^3 is located 1.34 Å from the uranyl oxygen and 1.82 Å from the uranium atom, along with a second peak of 2.25 e/Å^3 located trans to the 4.17 e/Å^3 peak across the uranium atom, suggesting the oxygen atoms of the uranyl group form a disordered crystallographic domain. No twinning was identified, and several different crystals were screened but the residual electron density was present in each structure solution.

Table 1. Crystal Data and Structure Refinement.

Formula	**$K_{1.78}Na_{1.22}[(UO_2)BSi_4O_{12}]$**
space group	*Cmce*
formula weight (g/mol)	682.77
temperature (K)	301(2)
a (Å)	15.5471(19)
b (Å)	14.3403(17)
c (Å)	11.7315(15)
volume (Å^3)	2615.5(6)
Z	8
density (g cm^{-3})	3.468
crystal dimensions (mm^3)	0.04 × 0.03 × 0.02
absorption coefficient (mm^{-1})	13.460
data collection and refinement	
collected reflections	72,412
independent reflections	2963
R_{int}	0.0341
refined restraints/parameters	1/120
goodness-of-fit on F^2	1.251
final *R* indices [$I > 2\sigma(I)$]	R_1 = 0.0356 wR_2 = 0.0678
final *R* indices (all data)	R_1 = 0.0376 wR_2 = 0.0686
largest diff. peak and hole (e$^-$/Å^3)	4.154 and −2.158

Single crystal X-ray data were also collected on the large crystals obtained from initial reactions utilizing KOH pellets rather than KOH stock solution, and refinement of the structure suggested a marginal difference in composition, $K_{1.7}Na_{1.3}[(UO_2)BSi_4O_{12}]$, although with poor refinement statistics (Table S1). Similar to $K_{1.8}Na_{1.2}[(UO_2)BSi_4O_{12}]$, residual electron density was also observed in the structure solution of $K_{1.7}Na_{1.3}[(UO_2)BSi_4O_{12}]$; however, only a single large peak of 10.35 e/Å^3 located 1.33 Å from the uranyl oxygen and 1.94 Å from the uranium atom was observed. Several different crystals were screened, and the same result was obtained in each case. The residual electron density persisted in data collected at low temperature as well as in structure solutions obtained in lower symmetry space groups, and no twinning was identified.

2.4. Topological Analysis

The ToposPro software package (Blatov, Shevchenko, Samara, Russia) was used to perform crystal structure analysis [44,45]. The ADS program was used to obtain underlying nets using the standard structure simplification procedure [46].

2.5. Powder X-ray Diffraction

Powder X-ray diffraction (PXRD) measurements were performed on a Bruker D2 Phaser diffractometer (Cu Kα radiation, λ = 1.54184 Å) equipped with a LYNXEYE XE-T detector. Data were collected over a 2θ range of 5–65° with a step size of 0.04°. PXRD data confirmed the phase purity of the obtained samples.

2.6. Spectroscopy

Raman spectroscopy measurements were performed on a Horiba XploraPLUS Raman microscope (Horiba, Kyoto, Japan) that was used to acquire spectra over the range of 525 to 950 cm^{-1} with a 638 nm laser as the excitation source. Scans were performed at 25% laser power and were collected on approximately 15 mg of powder sample that was deposited between two microscope slides and sealed on all sides with tape as containment during the measurement. Fourier-transform infrared spectroscopy data were collected on a powder sample using a PerkinElmer Spectrum 100 FT-IR spectrometer (PerkinElmer, Waltham, MA, United States) in the range of 650 to 4000 cm^{-1}.

Extended X-ray absorption fine structure (EXAFS) measurements were made using the MRCAT beamline, sector 10-BM-A,B at the Advanced Photon Source [47]. Measurements were made using the uranium L_{III} edge at 17.16 keV in transmission. Measurements were made for the new uranium borosilicate phase of interest and also for γ-UO_3 and α-U_3O_8 as standards. Data analysis was performed using the Athena and Artemis programs from the Demeter package [48] with a *k* weight of 3 and usable data range to 12.5 Å^{-1}.

2.7. Thermal Properties

Thermogravimetric and differential thermal analysis (TGA/DTA) measurements were performed on a polycrystalline powder sample using a TA SDT Q600 TGA (TA Instruments, New Castle, DE, Unites States). The sample was heated from room temperature to 800 °C under a flow of nitrogen gas at a purge rate of 100 mL per minute, and the resulting powder was analyzed by PXRD for phase identification after heating.

2.8. First Principles Calculations

We performed first principles calculations to carry out geometry optimizations in the form of density functional theory (DFT), using the Vienna Ab-initio Package (VASP) planewave code (VASP Software GmbH, Vienna, Austria) [49,50] generalized gradient approximation of Perdew, Burke and Ernzerhof (PBE) [51] and projector augmented wave (PAW) method [52,53]. Spin-polarized calculations were performed with 520 eV cut-off energy for the plane wave basis set, 10^{-4} eV energy convergence criteria and $3 \times 3 \times 3$ *k*-point mesh. The ground state geometries at 0 K were optimized by relaxing the cell volume, atomic positions, and cell symmetry until the maximum force on each atom

was less than 0.01 eV/Å. Implementation of Hubbard U correction of 4.0 eV for uranium f-orbitals resulted in similar optimized geometries.

3. Results and Discussion

3.1. Synthesis

Many factors are known to influence crystal growth in supercritical hydrothermal synthesis, including pH, temperature and pressure, mineralizer type, reactant solubilities, solution redox potential, reaction container type, etc. [54,55]. While there is valuable information to be gleaned from analysis of the reaction processes occurring in these conditions, such studies are often precluded by the presence of soluble intermediate species [56]. In the absence of the ability to perform mechanistic studies, part of our investigations of this system aimed to identify key factors dictating phase formation. Our findings indicated that the two predominating factors influencing the formation of $K_{1.8}Na_{1.2}[(UO_2)BSi_4O_{12}]$ are reaction dwell time and KOH concentration.

The optimal reaction time was determined to be 48 h, where shorter reaction times resulted in lower yields of $K_{1.8}Na_{1.2}[(UO_2)BSi_4O_{12}]$ and instead favored the formation of the co-crystallizing phases $Na_7UO_2(UO)_2(UO_2)_2Si_4O_{16}$ [39] and $K(UO)Si_2O_6$ [17]. Longer reaction times did not result in appreciable increase in yield or larger single crystals of $K_{1.8}Na_{1.2}[(UO_2)BSi_4O_{12}]$. The discrepancy between the products obtained from reactions beginning with KOH pellets versus KOH stock solution served as an indication of the relatively narrow range of conditions in which $K_{1.8}Na_{1.2}[(UO_2)BSi_4O_{12}]$ will form, where phase formation did not occur in reactions with KOH concentrations greater than 1.5 M. The optimal concentration range was determined to be approximately 0.5–1.5 M.

3.2. Structure Description

$K_{1.8}Na_{1.2}[(UO_2)BSi_4O_{12}]$ crystallizes in the centrosymmetric orthorhombic space group *Cmce* with lattice parameters a = 15.5471(19) Å, b = 14.3403(17) Å, c = 11.7315(15) Å, and V = 2615.5(6) Å^3. The asymmetric unit consists of one uranium atom, four potassium atoms, one sodium atom, two silicon atoms, one boron atom, and nine oxygen atoms. The structure is composed of isolated UO_6 octahedra that are coordinated through vertex-sharing of the equatorial oxygen atoms to $[BSi_4O_{12}]^{5-}$ chains, forming a framework with channels in which disordered Na^+ and K^+ cations reside (Figure 1). The borosilicate chains are made up of BO_4 and SiO_4 tetrahedra that run parallel to the c axis, where each BO_4 tetrahedron shares all four vertices with SiO_4 tetrahedra within the chain and each SiO_4 tetrahedron shares vertices with two adjacent SiO_4 tetrahedra, one BO_4 tetrahedron, and a distorted UO_6 octahedron. A table of selected interatomic distances is provided in the supporting information in Table S2.

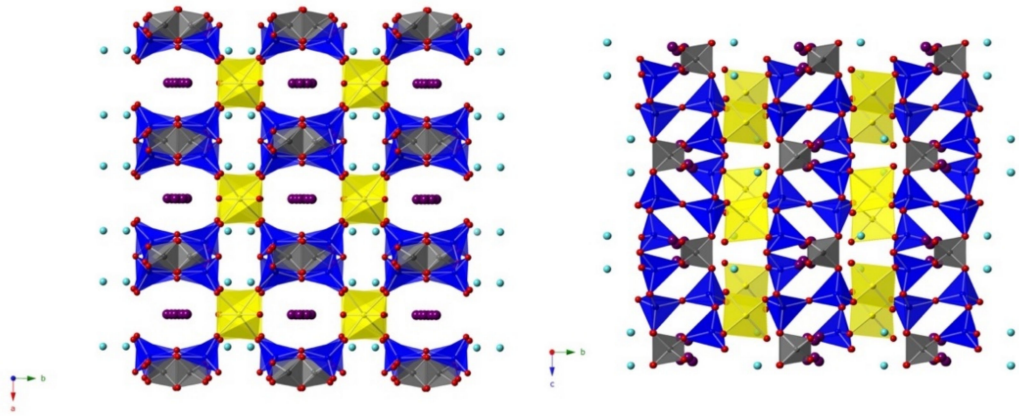

Figure 1. The three-dimensional $[(UO_2)BSi_4O_{12}]^{3-}$ framework is shown, where yellow octahedra represent UO_6 groups, gray tetrahedra are BO_4 groups, blue tetrahedra are SiO_4 groups, and purple and light blue spheres are K^+ cations and disordered Na^+/K^+, respectively.

The fundamental building block (FBB) of the borosilicate chain, $[BSi_4O_{12}]^{5-}$, is composed of four SiO_4 tetrahedra and one BO_4 tetrahedron that are connected through vertex-sharing, as shown in Figure 2a. The borosilicate FBB is an open-branched dreier-single ring that may be described as 5□:<4□>□ according to the notation proposed by Burns, Grice, and Hawthorne [57,58]. The simplified underlying net of the borosilicate chain topology is shown in Figure 2b. A variety of borosilicate units have been observed in non-uranyl compounds [31–36]; to the best of our knowledge, $K_{1.8}Na_{1.2}[(UO_2)BSi_4O_{12}]$ represents the first example of a compound containing $[BSi_4O_{12}]^{5-}$ units.

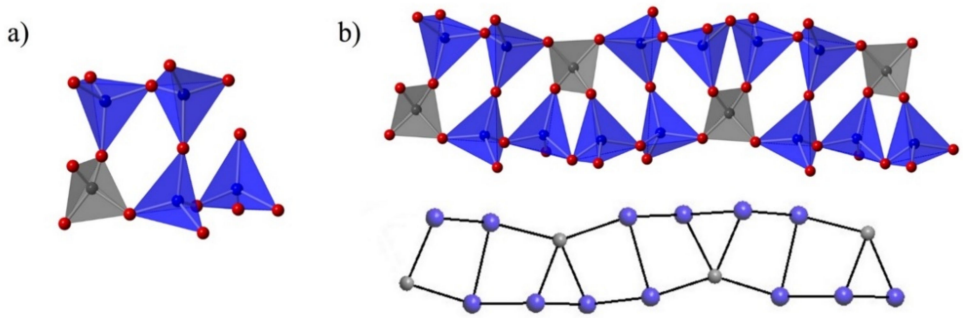

Figure 2. (**a**) The $[BSi_4O_{12}]^{5-}$ FBB of the borosilicate chain is shown and (**b**) a simplified net with BO_4 and SiO_4 tetrahedra shown as nodes within the chain.

Within the larger voids of the $[(UO_2)BSi_4O_{12}]^{3-}$ framework, K^+ cations are disordered over three sites that have a combined total occupancy of one, whereas the smaller channels contain disordered Na^+/K^+ cations located on a single site staggered between UO_6 octahedra, with occupancies of Na^+ and K^+ refining to 0.61 and 0.39, respectively. It was expected that larger alkali cations could be incorporated into the structure considering the extensive disorder of the K^+ cations in the large channels of the framework; however, attempts to synthesize the Rb and Cs analogs were unsuccessful.

The U-O bond lengths within the distorted UO_6 octahedra are typical, with the equatorial bond distances ranging from 2.233(2) to 2.245(3) Å and axial uranyl U(1)–O(1) and U(1)–O(2) bond distances of 1.819(4) and 1.813(4) Å, respectively. The bond valence sum (BVS) at the uranium site, using the parameters r_0 = 2.051 and B = 0.519, was calculated to be 5.93, which is consistent with U(VI). In the structure of $K_{1.7}Na_{1.3}[(UO_2)BSi_4O_{12}]$, the UO_6 equatorial and uranyl U(1)–O(2) bond distances are equivalent to those of $K_{1.8}Na_{1.2}[(UO_2)BSi_4O_{12}]$ within estimated standard deviations. The presence of the single large residual electron density peak (10.35 e/Å^3) located 1.33 Å from the uranyl oxygen O(1) and 1.94 Å from U(1), prompted us to consider the residual electron density as a possible oxygen atom. Assigning the peak as an oxygen atom and freely refining the occupancies of both the assigned oxygen site and the uranyl O(1) atom resulted in a partial occupancy of approximately 0.40 for the assigned oxygen site and full occupancy of O(1), constituting a possible O_2^{2-} peroxo group in lieu of a single uranyl oxygen (Figure 3). Using this model that takes into account the coordination of a peroxo group to the uranium atom, the BVS at the uranium site was calculated to be 6.67. Selected interatomic distances for $K_{1.7}Na_{1.3}[(UO_2)BSi_4O_{12}]$ are provided in Table S3.

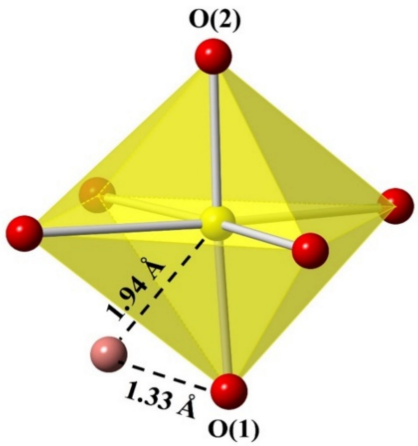

Figure 3. Residual electron density near the uranium atom and uranyl oxygen O(1) can be refined as a partially occupied oxygen (shown in light pink), resulting in a highly unusual coordination environment in which a peroxo group is coordinated to uranium along the axial direction.

While many uranyl peroxo compounds are known [59–64], reported examples are characterized by peroxo interactions existing within the equatorial plane; none that exhibit peroxo interactions along the axial direction have been reported. Furthermore, O-O bond lengths in uranyl peroxo compounds typically range between about 1.45 to 1.52 Å [65], and thus, the significantly shorter peroxo bond in this model (1.33 Å) warrants some skepticism. As an alternative to a peroxo group, the observed residual electron density might simply be an artifact from an unknown crystal defect, possibly relating to the incorporation of slightly more Na^+ on the disordered Na^+/K^+ site in $K_{1.7}Na_{1.3}[(UO_2)BSi_4O_{12}]$ than in $K_{1.8}Na_{1.2}[(UO_2)BSi_4O_{12}]$. Given the novelty of such a coordination environment for uranium, as well as this possibility of a crystal defect, further analysis was needed to either confirm or reject the peroxo structure model.

3.3. Spectroscopy

In order to probe for a peroxo group in the structure of $K_{1.7}Na_{1.3}[(UO_2)BSi_4O_{12}]$, Raman spectroscopy was performed. Shown in Figure 4, the predominating feature in the Raman spectrum is a band at 776 cm^{-1}, corresponding to the symmetric stretching of the uranyl moiety. This is consistent with the uranyl bond lengths determined from the single crystal X-ray data [66]. A few weak bands are observed in the spectrum between 548 to 744 cm^{-1} and are attributable to BO_4 and SiO_4 bending modes [34,67]. For η^2-peroxo complexes, the O-O symmetric stretching is normally observed as a strong band near 870 cm^{-1} [68], although this band has been observed to occur anywhere in the range of approximately 830 to 880 cm^{-1} in the spectra of uranyl peroxo compounds [69,70]. This region is bare in the Raman spectrum of $K_{1.7}Na_{1.3}[(UO_2)BSi_4O_{12}]$, with the exception of a weak band centered at approximately 830 cm^{-1}. Even in the case of a partially occupied peroxo group, it is expected that a band corresponding to the symmetric stretching mode would be fairly intense, thus we attribute the weak band at 830 cm^{-1} to the antisymmetric stretching of the uranyl moiety [16,71].

The IR spectrum of $K_{1.7}Na_{1.3}[(UO_2)BSi_4O_{12}]$ is complex, with significant overlap of the absorption bands of BO_4, SiO_4, and UO_2^{2+} observed. The spectrum, shown in Figure 5, exhibits two bands at 686 and 750 cm^{-1} that are attributed to the BO_4 and SiO_4 bending modes, in addition to antisymmetric and symmetric stretching absorptions of BO_4 and SiO_4 in the region of 750 to 1134 cm^{-1} [35,72]. The vibrational band at 901 cm^{-1} is assigned to the uranyl antisymmetric stretching [72,73].

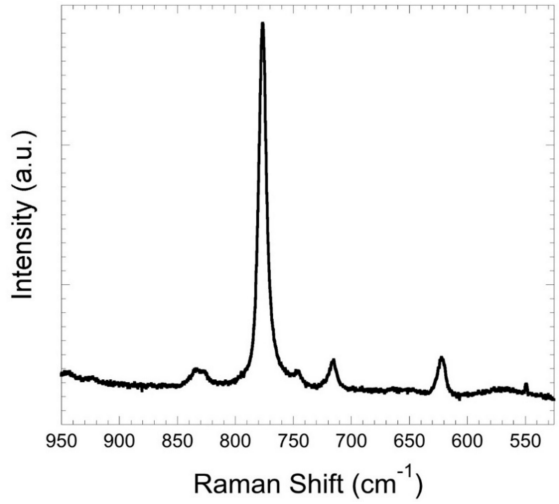

Figure 4. The Raman spectrum of $K_{1.7}Na_{1.3}[(UO_2)BSi_4O_{12}]$, which exhibits no bands in the range of 820 to 880 cm^{-1} where symmetric stretching of peroxo is expected to occur.

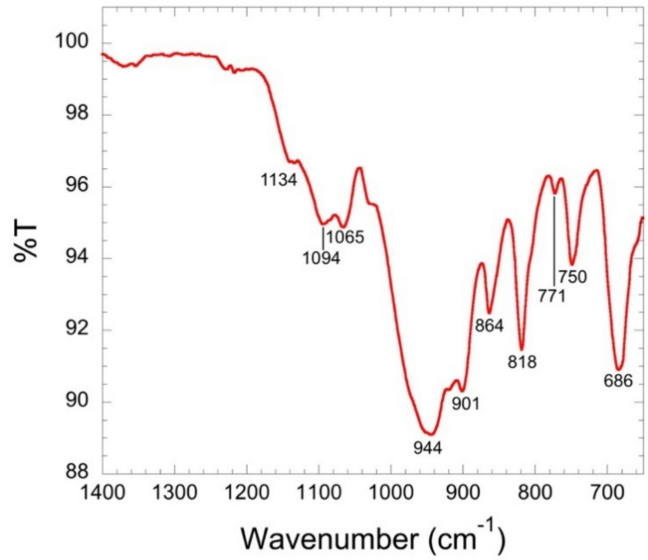

Figure 5. IR spectrum of $K_{1.7}Na_{1.3}[(UO_2)BSi_4O_{12}]$.

EXAFS was used to further probe the presence or absence of the peroxo oxygen in a 'side-on' configuration. The first coordination shell if the peroxo group is present has two oxygen ions at a distance of ~1.8 Å from the central uranium, with four additional oxygen ions at ~2.25 Å. The peroxo group oxygen is present at 1.95 Å, approximately halfway between the other oxygen distances. The structure model without the peroxo group has the same first-shell configuration but without the peroxo oxygen. Both structure models have nearly identical atom locations, with the primary difference being the presence of the peroxo oxygen, so it was only necessary to fit the first shell of the EXAFS data to distinguish between them.

First-shell fits were successful for the γ-UO_3 and α-U_3O_8 materials, and the fit to the new uranium borosilicate was good with or without the peroxo group, with R-values of 0.026 with the peroxo group and 0.022 without (Figure 6). For the model without the peroxo ion, the 4-parameter fit yielded sensible values with shifts of the oxygen ions of less than 0.01 Å and mean square relative displacement of 0.0020(7). However, the model for the peroxo group moved the peroxo oxygen to 2.13 Å while the initial model placed the oxygen ion at 1.95 Å. This result indicates that the peroxo oxygen is not a feature of the first coordination shell and that the model with only 6-fold coordination of the uranium ion is correct.

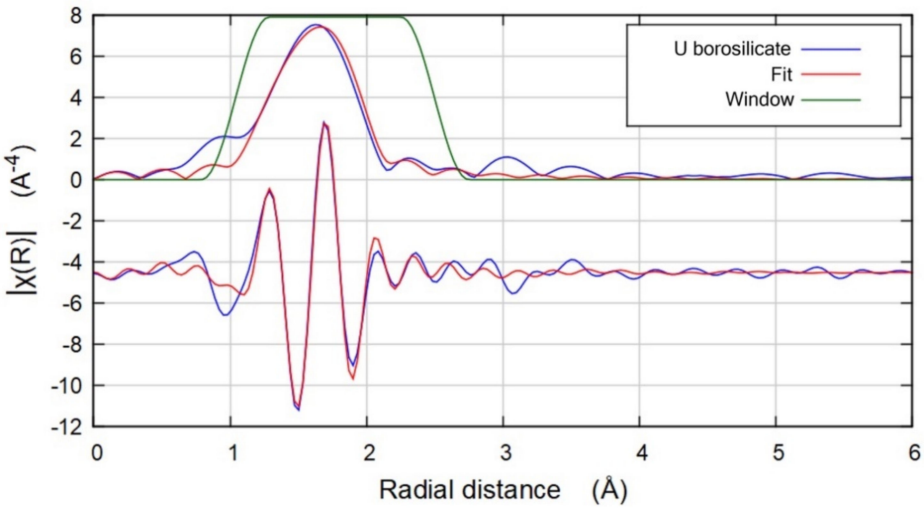

Figure 6. EXAFS first shell fit for uranium borosilicate. The real space magnitude and phase are shown with the first shell fit window.

3.4. Thermal Properties

TGA measurements were performed to assess the thermal behavior of $K_{1.7}Na_{1.3}[(UO_2)BSi_4O_{12}]$. It was expected that if the peroxo oxygen in question were present in the structure, a distinct weight loss step associated with loss of an oxygen would be observed. Based on a 40% occupancy of the peroxo oxygen as determined from structure refinements, a weight loss of approximately 0.9% was calculated. As shown in Figure 7, a total weight loss of only 0.45% was observed over the measurement range of 25 °C to 800 °C. PXRD patterns collected on TGA samples after heating revealed the material to be thermally stable up to 800 °C, with no significant changes observed in the patterns before and after heating (Figure 8). To verify the weight loss observed was not attributable to the loss of oxygen from a peroxo group, single crystal X-ray data were collected on a single crystal sample that was synthesized and subsequently heated to 800 °C. The residual electron density was still present in the structure model, and no other differences were observed in the structure model obtained for the sample heated post-synthesis.

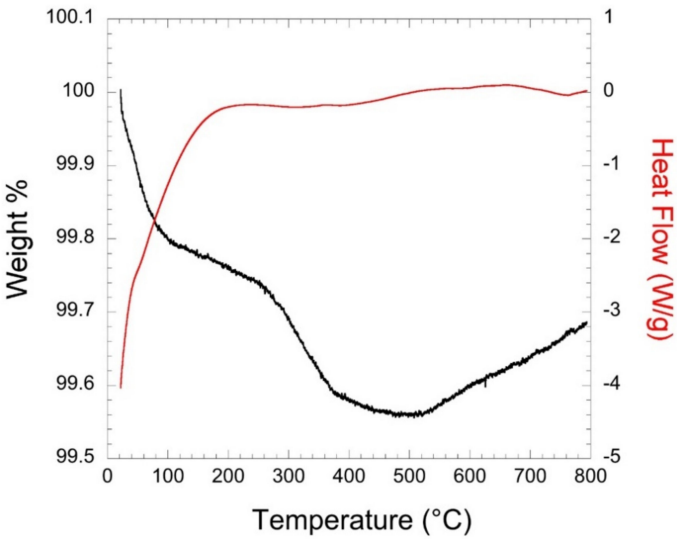

Figure 7. TGA/DTA data for $K_{1.7}Na_{1.3}[(UO_2)BSi_4O_{12}]$ collected from room temperature to 800 °C under a flow of nitrogen gas.

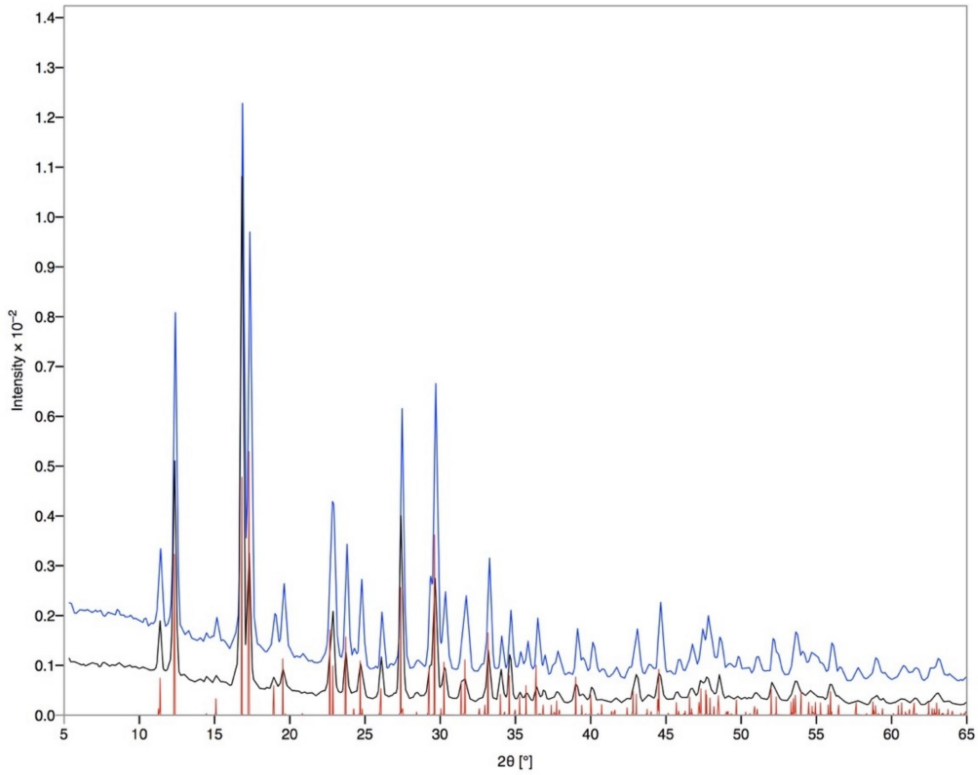

Figure 8. PXRD patterns of $K_{1.7}Na_{1.3}[(UO_2)BSi_4O_{12}]$ for TGA before (black) and after (blue) heating to 800 °C. The calculated pattern from the CIF is shown in red.

3.5. Energy Optimization Calculations

First principles calculations were used to optimize the geometry of the structure in order to determine the optimized U-O bond lengths of the uranyl oxygens and the peroxo oxygen. The results of the calculations are provided in Table 2. Three sets of calculations were performed in which the structure contained a fully occupied peroxo oxygen, a half-occupied peroxo oxygen, and no peroxo oxygen, allowing for a comparison of uranyl bond distances as a function of peroxo oxygen occupancy. The results of the calculations revealed the optimal U(1)–O_{peroxo} and U(1)–O(1) bond distances for the structure containing a half-occupied peroxo oxygen should be significantly elongated at approximately 2.17 and 2.16 Å, respectively. Only nominal differences in calculated bond lengths between the structure containing half- and fully occupied peroxo oxygen were determined, suggesting that any peroxo oxygen occupancy would result in elongated U-O bonds.

Table 2. DFT-Optimized Uranyl Bond Lengths in $K_{1.7}Na_{1.3}[(UO_2)BSi_4O_{12}]$ (Å).

U-O	Experimental	Calculated		
		Fully Occupied Peroxo	Half-Occupied Peroxo	No Peroxo
U(1)-O(1)	1.83	2.15	2.16	1.87
U(1)-O(2)	1.81	1.86	1.88	1.86
U(1)-O_{peroxo}	1.94	2.16	2.17	-

In comparison to the experimentally determined bond lengths, the calculated bond lengths for the structure containing no peroxo oxygen are still slightly elongated but are more consistent with the structure model obtained from single crystal X-ray data. Thus, in combined consideration of the structure, thermal, and spectroscopy data, the calculations better support the structure model exhibiting no axially coordinated peroxo.

4. Conclusions

In summary, hydrothermal synthesis methods were employed for the preparation of the first example of a uranyl borosilicate phase, $K_{1.8}Na_{1.2}[(UO_2)BSi_4O_{12}]$. The framework structure is made up of UO_6 octahedra connected by $[BSi_4O_{12}]^{5-}$ borosilicate chains containing BO_4 and SiO_4 tetrahedra, which constitutes a new borosilicate FBB. This highlights the structural diversity that is accessible in this new class of compounds, warranting further exploration of crystalline uranyl borosilicate compounds.

Successful synthesis of the phase was determined to occur under a relatively narrow set of conditions, where slight deviations in the KOH concentration of the reaction was initially thought to produce a related but distinct secondary phase with a possible partially occupied peroxo group in place of one of the uranyl oxygen atoms. The composition of this phase–with no peroxo accounted for–was determined to be $K_{1.7}Na_{1.3}[(UO_2)BSi_4O_{12}]$ from single crystal X-ray data. No evidence of O_2^{2-} symmetric stretching was observed in the Raman spectrum and first-shell fits of the EXAFS spectrum were consistent with a UO_6 coordination lacking a peroxo group. No loss of peroxo was observed upon heating the sample in TGA measurements, and in fact, no thermal decomposition was found to occur over the measurement range up to 800 °C. Furthermore, first principles calculations indicated the presence of a peroxo group should result in significantly longer U-O bonds than those determined experimentally. We therefore conclude the residual electron density in the structure models are attributable to a crystal defect and not a peroxo group.

Supplementary Materials: The following are available online at https://www.mdpi.com/article/10.3390/inorganics9040025/s1, Figure S1: Optical image of single crystals of $K_{1.7}Na_{1.3}[(UO_2)BSi_4O_{12}]$, Table S1: $K_{1.70}Na_{1.30}[(UO_2)BSi_4O_{12}]$ Crystal Data and Structure Refinement, Table S2: Selected Interatomic Distances for $K_{1.8}Na_{1.2}[(UO_2)BSi_4O_{12}]$ (Å), Table S3: Selected Interatomic Distances for $K_{1.7}Na_{1.3}[(UO_2)BSi_4O_{12}]$ (Å), checkCIF output file.

Author Contributions: Synthesis, data collection, and topological analysis were performed by K.A.P.; X-ray diffraction data collection and interpretation was performed by K.A.P., V.V.K., M.D.S., G.M. and H.-C.z.L.; EXAFS data interpretation and fittings were performed by S.T.M.; Raman data collection and interpretation was performed by K.A.P., T.W. and J.A.L.; first principles calculations were performed by V.V.K. The manuscript was written by K.A.P. with contributions from V.V.K. and S.T.M. and feedback from all the authors. All authors have read and agreed to the published version of the manuscript.

Funding: This work was supported as part of the Center for Hierarchical Waste Form Materials, an Energy Frontier Research Center funded by the U.S. Department of Energy (DOE), Office of Science, Basic Energy Sciences under Award No. DE-SC0016574 and by the South Carolina Smartstate Center for Strategic Approaches to the Generation of Electricity (SAGE). The EXAFS study was performed at MRCAT. MRCAT operations are supported by the DOE and the MRCAT member institutions. This research used resources of the Advanced Photon Source, a U.S. DOE Office of Science User Facility operated for the DOE Office of Science by Argonne National Laboratory under Contract No. DE-AC02-06CH11357.

Institutional Review Board Statement: Not applicable.

Informed Consent Statement: Not applicable.

Data Availability Statement: Accession code: CCDC 2035885. These data can be obtained free of charge via www.ccdc.cam.ac.uk/data_request/cif, or by emailing data_request@ccdc.cam.ac.uk, or by contacting The Cambridge Crystallographic Data Centre, 12 Union Road, Cambridge CB2 1EZ, UK; Fax +44 1223 336033.

Conflicts of Interest: The authors declare no conflict of interest.

References

1. National Research Council. *Waste Forms Technology and Performance*; Final Report by National Research Council of the National Academies; The National Academies Press: Washington, DC, USA, 2011.

2. Burns, P.C.; Olson, R.A.; Finch, R.J.; Hanchar, J.M.; Thibault, Y. $KNa_3(UO_2)_2(Si_4O_{10})_2(H_2O)_4$, a new compound formed during vapor hydration of an actinide-bearing borosilicate waste glass. *J. Nucl. Mater.* **2000**, *278*, 290–300. [CrossRef]
3. Wang, S.; Alekseev, E.V.; Ling, J.; Skanthakumar, S.; Soderholm, L.; Depmeier, W.; Albrecht-Schmitt, T.E. Neptunium diverges sharply from uranium and plutonium in crystalline borate matrixes: Insights into the complex behavior of the early actinides relevant to nuclear waste storage. *Angew. Chem. Int. Ed. Engl.* **2010**, *49*, 1263–1266. [CrossRef]
4. Weber, W.J.; Navrotsky, A.; Stefanovsky, S.V.; Vance, E.R.; Vernaz, E.Y. Materials science of high-level nuclear waste immobilization. *MRS Bull.* **2009**, *34*, 46–53. [CrossRef]
5. Zur Loye, H.-C.; Besmann, T.; Amoroso, J.; Brinkman, K.; Grandjean, A.; Henager, C.H.; Hu, S.; Misture, S.T.; Phillpot, S.R.; Shustova, N.B.; et al. Hierarchical Materials as Tailored Nuclear Waste Forms: A Perspective. *Chem. Mater.* **2018**, *30*, 4475–4488. [CrossRef]
6. Xu, Y.; Wen, Y.; Grote, R.; Amoroso, J.; Shuller Nickles, L.; Brinkman, K.S. A-site compositional effects in Ga-doped hollandite materials of the form $Ba_xCs_yGa_{2x+y}Ti_{8-2x-y}O_{16}$: Implications for Cs immobilization in crystalline ceramic waste forms. *Sci. Rep.* **2016**, *6*, 27412. [CrossRef]
7. Wang, S.; Alekseev, E.; Diwu, J.; Casey, W.; Phillips, B.; Depmeier, W.; Albrecht-Schmitt, T. NDTB-1: A Supertetrahedral Cationic Framework That Removes TcO_4^- from Solution. *Angew. Chem. Int. Ed.* **2010**, *49*, 1057–1060. [CrossRef] [PubMed]
8. Halasyamani, P.S.; Walker, S.M.; O'Hare, D. The First Open Framework Actinide Material $(C_4N_2H_{12})U_2O_4F_6$ (MUF-1). *J. Am. Chem. Soc.* **1999**, *121*, 7415–7416. [CrossRef]
9. Jackson, J.M.; Burns, P.C. A re-evaluation of the structure of weeksite, a uranyl silicate framework mineral. *Can. Mineral.* **2001**, *39*, 187–195. [CrossRef]
10. Wang, X.; Huang, J.; Liu, L.; Jacobson, A.J. The novel open-framework uranium silicates $Na_2(UO_2)(Si_4O_{10})\cdot 2.1H_2O$ (USH-1) and $RbNa(UO_2)(Si_2O_6)\cdot H_2O$ (USH-3). *J. Mater. Chem.* **2002**, *12*, 406–410. [CrossRef]
11. Chen, C.-S.; Kao, H.-M.; Lii, K.-H. $K_5(UO_2)_2[Si_4O_{12}(OH)]$: A uranyl silicate containing chains of four silicate tetrahedra linked by SiO···HOSi hydrogen bonds. *Inorg. Chem.* **2005**, *44*, 935–940. [CrossRef]
12. Liu, H.-K.; Chang, W.-J.; Lii, K.-H. High-Temperature, High-Pressure Hydrothermal Synthesis and Characterization of an Open-Framework Uranyl Silicate with Nine-Ring Channels: $Cs_2UO_2Si_{10}O_{22}$. *Inorg. Chem.* **2011**, *50*, 11773–11776. [CrossRef] [PubMed]
13. Liu, H.-K.; Peng, C.-C.; Chang, W.-J.; Lii, K.-H. Tubular Chains, Single Layers, and Multiple Chains in Uranyl Silicates: $A_2[(UO_2)Si_4O_{10}]$ (A = Na, K, Rb, Cs). *Cryst. Growth Des.* **2016**, *16*, 5268–5272. [CrossRef]
14. Morrison, G.; Tran, T.T.; Halasyamani, P.S.; zur Loye, H.-C. $K_8(K_5F)U_6Si_8O_{40}$: An Intergrowth Uranyl Silicate. *Inorg. Chem.* **2016**, *55*, 3215–3217. [CrossRef]
15. Morrison, G.; Smith, M.D.; zur Loye, H.-C. Understanding the Formation of Salt-Inclusion Phases: An Enhanced Flux Growth Method for the Targeted Synthesis of Salt-Inclusion Cesium Halide Uranyl Silicates. *J. Am. Chem. Soc.* **2016**, *138*, 7121–7129. [CrossRef]
16. Li, H.; Kegler, P.; Bosbach, D.; Alekseev, E.V. Hydrothermal Synthesis, Study, and Classification of Microporous Uranium Silicates and Germanates. *Inorg. Chem.* **2018**, *57*, 4745–4756. [CrossRef]
17. Chen, C.-S.; Lee, S.-F.; Lii, K.-H. $K(UO)Si_2O_6$: A pentavalent-uranium silicate. *J. Am. Chem. Soc.* **2005**, *127*, 12208–12209. [CrossRef]
18. Wang, S.; Alekseev, E.V.; Stritzinger, J.T.; Depmeier, W.; Albrecht-Schmitt, T.E. Crystal chemistry of the potassium and rubidium uranyl borate families derived from boric acid fluxes. *Inorg. Chem.* **2010**, *49*, 6690–6696. [CrossRef] [PubMed]
19. Wang, S.; Alekseev, E.V.; Stritzinger, J.T.; Depmeier, W.; Albrecht-Schmitt, T.E. How are centrosymmetric and noncentrosymmetric structures achieved in uranyl borates? *Inorg. Chem.* **2010**, *49*, 2948–2953. [CrossRef]
20. Wang, S.; Alekseev, E.V.; Ling, J.; Liu, G.; Depmeier, W.; Albrecht-Schmitt, T.E. Polarity and Chirality in Uranyl Borates: Insights into Understanding the Vitrification of Nuclear Waste and the Development of Nonlinear Optical Materials. *Chem. Mater.* **2010**, *22*, 2155–2163. [CrossRef]
21. Wang, S.; Alekseev, E.V.; Stritzinger, J.T.; Liu, G.; Depmeier, W.; Albrecht-Schmitt, T.E. Structure–Property Relationships in Lithium, Silver, and Cesium Uranyl Borates. *Chem. Mater.* **2010**, *22*, 5983–5991. [CrossRef]
22. Wu, S.; Wang, S.; Polinski, M.; Beermann, O.; Kegler, P.; Malcherek, T.; Holzheid, A.; Depmeier, W.; Bosbach, D.; Albrecht-Schmitt, T.E.; et al. High structural complexity of potassium uranyl borates derived from high-temperature/high-pressure reactions. *Inorg. Chem.* **2013**, *52*, 5110–5118. [CrossRef]
23. Hao, Y.; Klepov, V.V.; Murphy, G.L.; Modolo, G.; Bosbach, D.; Albrecht-Schmitt, T.E.; Kennedy, B.J.; Wang, S.; Alekseev, E.V. Influence of Synthetic Conditions on Chemistry and Structural Properties of Alkaline Earth Uranyl Borates. *Cryst. Growth Des.* **2016**, *16*, 5923–5931. [CrossRef]
24. Hao, Y.; Klepov, V.V.; Kegler, P.; Modolo, G.; Bosbach, D.; Albrecht-Schmitt, T.E.; Wang, S.; Alekseev, E.V. Synthesis and Study of the First Zeolitic Uranium Borate. *Cryst. Growth Des.* **2018**, *18*, 498–505. [CrossRef]
25. Wu, S.; Polinski, M.J.; Malcherek, T.; Bismayer, U.; Klinkenberg, M.; Modolo, G.; Bosbach, D.; Depmeier, W.; Albrecht-Schmitt, T.E.; Alekseev, E.V. Novel fundamental building blocks and site dependent isomorphism in the first actinide borophosphates. *Inorg. Chem.* **2013**, *52*, 7881–7888. [CrossRef]
26. Hao, Y.; Murphy, G.L.; Bosbach, D.; Modolo, G.; Albrecht-Schmitt, T.E.; Alekseev, E.V. Porous Uranyl Borophosphates with Unique Three-Dimensional Open-Framework Structures. *Inorg. Chem.* **2017**, *56*, 9311–9320. [CrossRef] [PubMed]

27. Hao, Y.C.; Hu, C.L.; Xu, X.; Kong, F.; Mao, J.G. $SrGe_2B_2O_8$ and $Sr_3Ge_2B_6O_{16}$: Novel strontium borogermanates with three-dimensional and layered anionic architectures. *Inorg. Chem.* **2013**, *52*, 13644–13650. [CrossRef]
28. Wu, S.; Beermann, O.; Wang, S.; Holzheid, A.; Depmeier, W.; Malcherek, T.; Modolo, G.; Alekseev, E.V.; Albrecht-Schmitt, T.E. Synthesis of uranium materials under extreme conditions: $UO_2[B_3Al_4O_{11}(OH)]$, a complex 3D aluminoborate. *Chem. Eur. J.* **2012**, *18*, 4166–4169. [CrossRef]
29. Klepov, V.V.; Juillerat, C.A.; Alekseev, E.V.; zur Loye, H.-C. Overstepping Löwenstein's Rule—A Route to Unique Aluminophosphate Frameworks with Three-Dimensional Salt-Inclusion and Ion Exchange Properties. *Inorg. Chem.* **2019**, *58*, 724–736. [CrossRef]
30. Mutailipu, M.; Poeppelmeier, K.R.; Pan, S. Borates: A Rich Source for Optical Materials. *Chem. Rev.* **2021**, *121*, 1130–1202. [CrossRef]
31. Lin, X.; Zhang, F.; Pan, S.; Yu, H.; Zhang, F.; Dong, X.; Han, S.; Dong, L.; Bai, C.; Wang, Z. $Ba_4(BO_3)_3(SiO_4)\cdot Ba_3X$ (X = Cl, Br): New salt-inclusion borosilicate halides as potential deep UV nonlinear optical materials. *J. Mater. Chem. C* **2014**, *2*, 4257. [CrossRef]
32. Miao, Z.; Yang, Y.; Wei, Z.; Yang, Z.; Yu, S.; Pan, S. $NaCa_5BO_3(SiO_4)_2$ with Interesting Isolated $[BO_3]$ and $[SiO_4]$ Units in Alkali- and Alkaline-Earth-Metal Borosilicates. *Inorg. Chem.* **2019**, *58*, 3937–3943. [CrossRef]
33. Heyward, C.C.; McMillen, C.D.; Kolis, J.W. Hydrothermal Growth of Lanthanide Borosilicates: A Useful Approach to New Acentric Crystals Including a Derivative of Cappelenite. *Inorg. Chem.* **2014**, *54*, 905–913. [CrossRef] [PubMed]
34. Wu, H.; Yu, H.; Pan, S.; Huang, Z.; Yang, Z.; Su, X.; Poeppelmeier, K.R. $Cs_2B_4SiO_9$: A Deep-Ultraviolet Nonlinear Optical Crystal. *Angew. Chem. Int. Ed.* **2013**, *52*, 3406–3410. [CrossRef] [PubMed]
35. Heyward, C.; McMillen, C.D.; Kolis, J. Hydrothermal synthesis and structural analysis of new mixed oxyanion borates: $Ba_{11}B_{26}O_{44}(PO_4)_2(OH)_6$, $Li_9BaB_{15}O_{27}(CO_3)$ and $Ba_3Si_2B_6O_{16}$. *J. Solid State Chem.* **2013**, *203*, 166–173. [CrossRef]
36. Chang, L.-W.; Liu, H.-K.; Lii, K.-H. Flux synthesis and characterization of two barium hydroxyborosilicates with triple and single tetrahedral layers: $Ba_2[Si_3B_3O_{12}(OH)]$ and $Ba[Si_2BO_6(OH)]$. *J. Solid State Chem.* **2020**, *287*, 121331. [CrossRef]
37. Medvedev, A.G.; Mikhaylov, A.A.; Churakov, A.V.; Vener, M.V.; Tripol'skaya, T.A.; Cohen, S.; Lev, O.; Prikhodchenko, P.V. Potassium, Cesium, and Ammonium Peroxogermanates with Inorganic Hexanuclear Peroxo Bridged Germanium Anion Isolated from Aqueous Solution. *Inorg. Chem.* **2015**, *54*, 8058–8065. [CrossRef] [PubMed]
38. Manceau, A.; Gorshkov, A.I.; Drits, V.A. Structural chemistry of Mn, Fe, Co, and Ni in manganese hydrous oxides: Part II. Information from EXAFS spectroscopy and electron and X-ray diffraction. *Am. Mineral.* **1992**, *77*, 1144–1157.
39. Lee, C.-S.; Lin, C.-H.; Wang, S.-L.; Lii, K.-H. $[Na_7U^{IV}O_2(U^VO)_2(U^{V/VI}O_2)_2Si_4O_{16}]$: A mixed-valence uranium silicate. *Angew. Chem. Int. Ed.* **2010**, *49*, 4254–4256. [CrossRef]
40. *APEXIII Version 2016. 5-0, SAINT Version 7.60A, SADABS Version 2016/2*; Bruker Analytical X-ray Systems: Madison, WI, USA, 2016.
41. Sheldrick, G.M. SHELXT—Integrated space-group and crystal-structure determination. *Acta Cryst.* **2015**, *A71*, 3–8. [CrossRef]
42. Sheldrick, G.M. A short history of SHELX. *Acta Cryst.* **2008**, *A64*, 112–122. [CrossRef]
43. Spek, A.L. Single-crystal structure validation with the program PLATON. *J. Appl. Crystallogr.* **2003**, *36*, 7–13. [CrossRef]
44. Blatov, V.A.; Shevchenko, A.P.; Proserpio, D.M. Applied Topological Analysis of Crystal Structures with the Program Package ToposPro. *Cryst. Growth Des.* **2014**, *14*, 3576–3586. [CrossRef]
45. Blatov, V.A.; Shevchenko, A.P.; Serezhkin, V.N. Multipurpose Crystallochemical Analysis with the Program Package TOPOS. *IUCr CompComm Newslett.* **2006**, *7*, 4–38.
46. Alexandrov, E.V.; Blatov, V.A.; Kochetkov, A.V.; Proserpio, D.M. Underlying nets in three-periodic coordination polymers: Topology, taxonomy and prediction from a computer-aided analysis of the Cambridge Structural Database. *CrystEngComm* **2011**, *13*, 3947–3958. [CrossRef]
47. Kropf, A.J.; Katsoudas, J.; Chattopadhyay, S.; Shibata, T.; Lang, E.A.; Zyryanov, V.N.; Ravel, B.; McIvor, K.; Kemner, K.M.; Scheckel, K.G.; et al. The New MRCAT (Sector 10) Bending Magnet Beamline at the Advanced Photon Source. *AIP Conf. Proc.* **2010**, *1234*, 299–302. [CrossRef]
48. Ravel, B.; Newville, M. ATHENA, ARTEMIS, HEPHAESTUS: Data analysis for X-ray absorption spectroscopy using IFEFFIT. *J. Synchrotron Radiat.* **2005**, *12*, 537–541. [CrossRef]
49. Kresse, G.; Furthmüller, J. Efficiency of ab-initio total energy calculations for metals and semiconductors using a plane-wave basis set. *Comput. Mater. Sci.* **1996**, *6*, 15–50. [CrossRef]
50. Kresse, G. Efficient iterative schemes for ab initio total-energy calculations using a plane-wave basis set. *Phys. Rev. B* **1996**, *54*, 11169–11186. [CrossRef]
51. Perdew, J.P.; Burke, K.; Ernzerhof, M. Generalized gradient approximation made simple. *Phys. Rev. Lett.* **1997**, *78*, 1396–1399. [CrossRef]
52. Blöchl, P.E. Projector augmented-wave method. *Phys. Rev. B* **1994**, *50*, 17953–17979. [CrossRef]
53. Kresse, G. From ultrasoft pseudopotentials to the projector augmented-wave method. *Phys. Rev. B* **1999**, *59*, 1758–1775. [CrossRef]
54. Rabenau, A. The role of hydrothermal synthesis in materials science. *J. Mater. Educ.* **1988**, *10*, 543–591.
55. Stritzinger, J.T.; Alekseev, E.V.; Polinski, M.J.; Cross, J.N.; Eaton, T.M.; Albrecht-Schmitt, T.E. Further evidence for the stabilization of U(V) within a tetraoxo core. *Inorg. Chem.* **2014**, *53*, 5294–5299. [CrossRef]
56. McMillen, C.D.; Kolis, J.W. Hydrothermal synthesis as a route to mineralogically-inspired structures. *Dalton Trans.* **2016**, *45*, 2772–2784. [CrossRef]

57. Burns, P.C.; Grice, J.D.; Hawthorne, F.C. Borate Minerals. I. Polyhedral Clusters and Fundamental Building Blocks. *Can. Mineral.* **1995**, *33*, 1131–1151.
58. Ewald, B.; Huang, Y.-X.; Kniep, R. Structural Chemistry of Borophosphates, Metalloborophosphates, and Related Compounds. *Z. Anorg. Allg. Chem.* **2007**, *633*, 1517–1540. [CrossRef]
59. Qiu, J.; Ling, J.; Sieradzki, C.; Nguyen, K.; Wylie, E.M.; Szymanowski, J.E.S.; Burns, P.C. Expanding the Crystal Chemistry of Uranyl Peroxides: Four Hybrid Uranyl-Peroxide Structures Containing EDTA. *Inorg. Chem.* **2014**, *53*, 12084–12091. [CrossRef] [PubMed]
60. Qiu, J.; Ling, J.; Jouffret, L.; Thomas, R.; Szymanowski, J.E.S.; Burns, P.C. Water-soluble multi-cage super tetrahedral uranyl peroxide phosphate clusters. *Chem. Sci.* **2014**, *5*, 303–310. [CrossRef]
61. Zhang, Y.; Bhadbhade, M.; Price, J.R.; Karatchevtseva, I.; Collison, D.; Lumpkin, G.R. Kinetics vs. thermodynamics: A unique crystal transformation from a uranyl peroxo-nanocluster to a nanoclustered uranyl polyborate. *RSC Adv.* **2014**, *4*, 34244–34247. [CrossRef]
62. Thangavelu, S.G.; Cahill, C.L. Uranyl-Promoted Peroxide Generation: Synthesis and Characterization of Three Uranyl Peroxo $[(UO_2)_2(O_2)]$ Complexes. *Inorg. Chem.* **2015**, *54*, 4208–4221. [CrossRef]
63. Qiu, J.; Dembowski, M.; Szymanowski, J.E.S.; Toh, W.C.; Burns, P.C. Time-Resolved X-ray Scattering and Raman Spectroscopic Studies of Formation of a Uranium-Vanadium-Phosphorus-Peroxide Cage Cluster. *Inorg. Chem.* **2016**, *55*, 7061–7067. [CrossRef] [PubMed]
64. Dembowski, M.; Colla, C.A.; Hickam, S.; Oliveri, A.F.; Szymanowski, J.E.S.; Oliver, A.G.; Casey, W.H.; Burns, P.C. Hierarchy of Pyrophosphate-Functionalized Uranyl Peroxide Nanocluster Synthesis. *Inorg. Chem.* **2017**, *56*, 5478–5487. [CrossRef]
65. Qiu, J.; Spano, T.L.; Dembowski, M.; Kokot, A.M.; Szymanowski, J.E.; Burns, P.C. Sulfate-Centered Sodium-Icosahedron-Templated Uranyl Peroxide Phosphate Cages with Uranyl Bridged by μ-η^1:η^2 Peroxide. *Inorg. Chem.* **2017**, *56*, 1874–1880. [CrossRef] [PubMed]
66. Bartlett, J.R. On the determination of uranium-oxygen bond lengths in dioxouranium(VI) compounds by Raman spectroscopy. *J. Mol. Struct.* **1989**, *193*, 295–300. [CrossRef]
67. Frost, R.L.; Bouzaid, J.M.; Martens, W.N.; Reddy, B.J. Raman spectroscopy of the borosilicate mineral ferroaxinite. *J. Raman Spectrosc.* **2007**, *38*, 135–141. [CrossRef]
68. Bastians, S.; Crump, G.; Griffith, W.P.; Withnall, R. Raspite and studtite: Raman spectra of two unique minerals. *J. Raman Spectrosc.* **2004**, *35*, 726–731. [CrossRef]
69. Dembowski, M.; Bernales, V.; Qiu, J.; Hickam, S.; Gaspar, G.; Gagliardi, L.; Burns, P.C. Computationally-Guided Assignment of Unexpected Signals in the Raman Spectra of Uranyl Triperoxide Complexes. *Inorg. Chem.* **2017**, *56*, 1574–1580. [CrossRef]
70. McGrail, B.T.; Sigmon, G.E.; Jouffret, L.J.; Andrews, C.R.; Burns, P.C. Raman Spectroscopic and ESI-MS Characterization of Uranyl Peroxide Cage Clusters. *Inorg. Chem.* **2014**, *53*, 1562–1569. [CrossRef] [PubMed]
71. Frost, R.L.; Čejka, J.; Weier, M.L.; Martens, W. Molecular structure of the uranyl silicates—A Raman spectroscopic study. *J. Raman Spectrosc.* **2006**, *37*, 538–551. [CrossRef]
72. Frost, R.L.; Čejka, J.; Weier, M.L.; Martens, W.; Kloprogge, J.T. A Raman and infrared spectroscopic study of the uranyl silicates-weeksite, soddyite and haiweeite. *Spectrochim. Acta A* **2006**, *64*, 308–315. [CrossRef]
73. Faulques, E.; Kalashnyk, N.; Massuyeau, F.; Perry, D.L. Spectroscopic markers for uranium phosphates: A vibronic study. *RSC Adv.* **2015**, *5*, 71219–71227. [CrossRef]